Testing chemistry-climate models' regulation of tropical lower-stratospheric water vapor

Kevin M. Smalley[1], Andrew E. Dessler[1], Slimane Bekki[2], Makoto Deushi[3], Marion Marchand[2], Olaf Morgenstern[4], David A. Plummer[5], Kiyotaka Shibata[6], Yousuke Yamashita[7,8], and Guang Zeng[4]

[1]Department of Atmospheric Science, Texas A&M, College Station, Texas, USA.
[2]LATMOS, Institut Pierre Simon Laplace (IPSL), Paris, France
[3]Meteorological Research Institute, 1-1 Nagamine, Tsukuba, Ibaraki 305-0052, Japan
[4]National Institute of Water and Atmospheric Research (NIWA), Wellington, New Zealand
[5]Canadian Centre for Climate Modelling and Analysis, Environment and Climate Change Canada
[6]School of Environmental Science and Engineering, Kochi University of Technology
[7]National institute for Environmental Studies (NIES)
[8]Now at Japan Agency for Marine-Earth Science and Technology (JAMSTEC), Yokohama, Japan

Correspondence to: Andrew Dessler (adessler@tamu.edu)

Abstract. Climate models predict that tropical lower-stratospheric humidity will increase as the climate warms, with important implications for the chemistry and climate of the atmosphere. We analyze the trend in 21st-century simulations from 12 state-of-the-art chemistry-climate models (CCMs) using a linear regression model to determine the factors driving the trends. Within CCMs, warming of the troposphere primarily drives the long-term trend in stratospheric humidity. This is partially offset in most CCMs by an increase in the strength of the Brewer-Dobson circulation, which tends to cool the tropical tropopause layer (TTL). We also apply the regression model to individual decades from the 21st century CCM runs and compare them to observations. Many of the CCMs, but not all, compare well with observations, lending credibility to their predictions. One notable deficiency in most CCMs is that they underestimate the impact of the quasi-biennial oscillation on lower-stratospheric humidity. Our analysis provides a new and potentially superior way to evaluate model trends in lower-stratospheric humidity.

1 Introduction

Stratospheric water vapor is well-known to be a greenhouse gas (e.g. Manabe and Wetherald, 1967; Forster and Shine, 1999; Solomon et al., 2010; Maycock et al., 2014), so increasing it will lead to additional warming of the climate system. Because of this, understanding the processes that control the humidity of air entering the tropical lower stratosphere (hereafter $[H_2O]_{entry}$) has been a high priority of the scientific community since Brewer (1949) first described the stratospheric circulation.

It is now well established that the fundamental control over $[H_2O]_{entry}$ comes from the coldest temperatures found in the tropical tropopause layer (TTL) (Fueglistaler et al., 2009b), frequently referred to as the Lagrangian dry point, and that variability in these temperatures translates into variability in $[H_2O]_{entry}$. The most well-known example of this is the so-called "tape recorder," in which the seasonal cycle in TTL temperatures is imprinted on tropical stratospheric water vapor (Mote et al., 1996).

On interannual time scales, variability in $[H_2O]_{entry}$ originates from processes such as the Brewer-Dobson Circlation (BDC) (Randel et al., 2006; Castanheira et al., 2012; Fueglistaler et al., 2014; Gilford et al., 2016) and the quasi-biennial oscillation (QBO) (O'Sullivan and Dunkerton, 1997; Randel et al., 1998; Dunkerton, 2001; Fueglistaler and Haynes, 2005; Choiu et al., 2006; Liang et al., 2011; Castanheira et al., 2012; Khosrawi et al., 2013; Kawatani et al., 2014; Tao et al., 2015). More recently, Dessler et al. (2013, 2014) suggested that the temperature of the troposphere also exerts an influence on $[H_2O]_{entry}$. This was based on the well-established observation that models predict a warming TTL during global warming [e.g., Gettelman et al. 2010]; in the models analyzed here (described in the next section) the tropospheric temperature is highly correlated with TTL temperatures, with a mean correlation of 0.91. There are good physical reasons for this connection [Lin et al., 2017]. In addition, Dessler et al. [2016] demonstrated in two CCMs that a warming climate also caused increased amounts of water to be directly injected into the stratosphere via deep convection, providing another mechanism for tropospheric temperature to affect $[H_2O]_{entry}$.

Putting these factors together, Dessler et al. (2013, 2014) demonstrated that observed $[H_2O]_{entry}$ anomalies could be accurately reproduced with a simple linear model:

$$[H_2O]_{entry} = \beta_0 + \beta_{\Delta T}\Delta T + \beta_{BDC}BDC + \beta_{QBO}QBO + \epsilon \tag{1}$$

Where ΔT is the temperature of the troposphere, BDC is the strength of the Brewer-Dobson circulation, QBO represents the phase of the QBO, and epsilon is the residual. Dessler et al. (2013) analyzed the 21st century trend in one chemistry-climate model (hereafter, CCM; they are similar to general circulation models, but with a more realistic stratosphere and higher vertical resolution in the TTL) and found that the regression model worked well in reproducing the CCM's $[H_2O]_{entry}$ trend over the 21st century. They concluded that the increase in $[H_2O]_{entry}$ was driven by the increase in tropospheric temperatures, which was partially offset by a strengthening BDC.

Dessler et al. (2013)'s regression method provides a novel way to examine the regulation of $[H_2O]_{entry}$ in CCMs and compare it to observations. The purpose of this paper is to use this technique to examine a set of CCMs, with the goal of providing insight into the realism of the models.

2 Models

We analyze model output from 7 CCMs participating in Phase 2 of the Chemistry-Climate Model Validation Project (CCMVal-2) (Morgenstern et al. (2010); SPARC (2010)) and output from 5 CCMs participating in Phase 1 of the Chemistry-Climate Model Initiative (CCMI-1) (Morgenstern et al. (2017)). Table 1 lists the model specifics and documentation.

We use simulations from the REF-B2 scenario of CCMVal-2. In this scenario, greenhouse gas concentrations during the 21st century come from the A1B scenario, which lies in the middle of the SRES scenarios (IPCC, 2001). Ozone-depleting substances come from the halogen emission scenario A1 described by (WMO, 2007). CCMVal-2 specifics can be found in SPARC (2010) and Morgenstern et al. (2010). We use the refC2 scenario of the CCMI-1. In this scenario, greenhouse gas

concentrations come from the RCP 6.0 scenario (Meinshausen et al., 2011) and ozone-depleting substances come from the halogen emission scenario A1 described by WMO (2014). CCMI-1 model specifics can be found in Morgenstern et al. (2017). In order to maintain a consistent reference period between models, our analysis covers 2000-2097, which we will hereafter refer to as "the 21st century".

5　　For each model, we fit CCM $[H_2O]_{entry}$ using the multivariate linear regression (MLR) model described above. We use tropical average 80-hPa water vapor volume mixing ratio as a proxy for $[H_2O]_{entry}$ (all tropical averages in this paper are averages over 30°N-30°S). For our BDC index, we use 80-hPa diabatic heating rate (see Fueglistaler et al. (2009a) for details). The tropospheric temperature index is the 500-hPa tropical average temperature, and for the few CCMI-1 simulations that only produce variables on hybrid pressure levels (CMAM, CCSRNIES-MIROC3.2, and MRI-ESM1r1), we choose a hybrid

10　pressure level close to the 500-hPa pressure surface (See Table 1). All of these choices are similar to those used by Dessler et al. (2013, 2014).

　　For the QBO index, we take the standardized anomaly of equatorial 50-hPa zonal winds (anomalies in this paper are calculated by subtracting the mean seasonal cycle). By examining 21st century 50 hPa zonal winds (shown in supplement figures), we find that only 5 of the 12 models simulate a QBO (table 1). As a result, we do not expect the QBO to significantly impact

15　$[H_2O]_{entry}$ in many of the models.

　　The MLR returns the coefficients for each regressor in Equation 1, along with an uncertainty for each coefficient. Unless otherwise noted, we use 95%-confidence intervals in this paper. Autocorrelation in the residuals is accounted for in the uncertainties following Santer et al. (2000).

3　Century Analysis

20　We first analyze the long-term trend in $[H_2O]_{entry}$ over the 21st century. To do this, we calculate annual average values of $[H_2O]_{entry}$ and perform a MLR against annual averages of the indices for BDC, QBO and ΔT. For consistency, all annual average time series have had the 2000-2010 mean subtracted out.

　　Figure 1 shows that the fits to most of the models generate adjusted R^2 values greater than 0.8. The NIWA-UKCA century MLR has the lowest adjusted R^2, with a value of approximately 0.6. Overall, this result confirms the result of Dessler et al.

25　(2013) that the regression model does an excellent job reproducing the models' $[H_2O]_{entry}$. Because we have left long-term trends in the time series, we will refer to this as the "trended analysis".

3.1　Detrended 21st Century

One concern with the trended analysis is that the $[H_2O]_{entry}$,BDC, and ΔT time series are all dominated by long-term trends. In such a case, an MLR may produce a high adjusted R^2 even if there is no actual relation between the variables. To eliminate

30　the influence of long-term trends on adjusted R^2, we detrend each variable using a Fourier Transform filter (Donnelly, 2006) to remove long-term variability (> 10 years). We then use the MLR on the detrended $[H_2O]_{entry}$ and the detrended indices. Detrending by removing the long-term linear trend yields similar results.

Figure 1 shows the adjusted R^2 for the detrended calculation. For most of the models, the adjusted R^2 for the detrended MLR is only slightly smaller than that for the trended one. This confirms that the long-term trends in the data tend to inflate the adjusted R^2, at least a bit, and also that the models' detrended variability are also well represented by the same linear model (Equation 1). Large differences do exist for some CCMs. For instance, the CCSRNIES trended century MLR captures approximately 90% of the variance in $[H_2O]_{entry}$, while the detrended century MLR only explains about 40% of detrended variance; the CNRM-CM5-3, NIWA-UKCA, and WACCM show something similar.

3.2   Physical Process Effects

The coefficients from the trended and detrended calculations are listed in Tables 2 and 3 respectively. The product of the regression coefficient and its index quantifies that process' impact on $[H_2O]_{entry}$. As an example, MRI $[H_2O]_{entry}$ increases by about 1.2 ppmv during the 21st century (Figure 2). The regression shows that this is the result of a large increase in $[H_2O]_{entry}$ due to ΔT increases (1.5 ppmv) that is offset by a strengthening BDC, which reduces $[H_2O]_{entry}$ by approximately 0.3 ppmv. The regression finds virtually no change in $[H_2O]_{entry}$ in response to the QBO.

Figure 3 shows that $[H_2O]_{entry}$ increases as ΔT increases in all models and that the ΔT regression coefficients are similar for both trended and detrended MLRs. The coefficient for individual models ranges from 0.1 to 0.6 ppmv K^{-1}, with an average of 0.32 ppmv K^{-1} and a standard deviation of 0.15 ppmv K^{-1}.

This figure also shows that the BDC coefficient is generally negative, meaning that a strengthening BDC reduces $[H_2O]_{entry}$. This is consistent with previous research, which showed that a stronger BDC reduces TTL temperatures and lower-stratospheric water vapor (Randel et al., 2006; Gilford et al., 2016). The coefficient for individual models ranges from -12. to 4.3 ppmv $(K/Day)^{-1}$, with an average of -3.55 ppmv $(K/Day)^{-1}$ and a standard deviation of 4.45 ppmv $(K/Day)^{-1}$. Two models (CNRM-CM5-3 and NIWA-UKCA) yield positive BDC coefficients, indicating potential problems with these models. And the MRI-ESMr1 produces, relative to other similar models, much larger BDC coefficients than MRI. This could explain why the detrended adjusted R^2 value for MRI-ESMr1 is so much smaller than that of MRI.

Figure 3 shows that all QBO regression coefficients are small, generally within $\pm$ 0.04 ppmv, with even the sign of the effect in doubt. Interestingly, one of the CCMs not simulating a QBO, CMAM-CCMI, produces the largest QBO regression coefficients of 0.082 $\pm$0.04 and 0.077 $\pm$0.04 ppmv for the trended and detrended calculations, respectively. Among CCMs that do simulate a QBO, the ensemble average QBO regression coefficient does not differ much from the same quantity (approximately 0 ppmv) for the other models. We will discuss this further in the next section.

We have also calculated the long-term linear trend of $[H_2O]_{entry}$ for each model, as well as the trend in each component of $[H_2O]_{entry}$, as determined by the multivariate fit (e.g., the trend in the components plotted in Fig. 2). We find that ΔT makes the largest contribution to the trend in $[H_2O]_{entry}$, with a smaller negative effect from the a strengthening BDC on $[H_2O]_{entry}$, and a trend of close to zero for the QBO (Figure 4).

To provide additional information about the relative contribution from the individual terms in eq. 1, we have also calculated standardized regression coefficients. To do this, we take each regression coefficient and multiply it by the standard deviation of the associated regressor index. The values are listed in tables 2 and 3 and they confirm that, in the trended calculations, ΔT is

the dominant cause of the trend in $[H_2O]_{entry}$. The BDC acts to reduce the trend, but its overall impact is much smaller than ΔT.

In the detrended calculations, the standardized ΔT regression coefficients are smaller than those from the trended calculations, while the magnitude of the BDC coefficients remains relatively constant. For variability associated with short-term variability, this suggests that the BDC is more important than ΔT. In all of our calculations, we find that the QBO has little impact on $[H_2O]_{entry}$. Again, we will discuss this further in the next section.

4 Decadal Analysis

Ideally, we would compare the results of the last section to observations. Unfortunately, we don't have 100 years of observations to test the models against. Instead, we will compare regressions of 10-year segments from the CCMs to regressions of 10-years of observations. This will help us evaluate how good the models are and provide us with an indication of how representative a single decade is.

Specifically, we split 21st century of each CCM run into 10 decades (2000-2010, 2010-2020, 2020-2030, 2040-2050, etc.) and fit each individual decade using the regression model (Equation 1). The regression calculation used on each 10-year segment is identical to the century analysis, except monthly averaged anomalies of all quantities are used instead of annual mean anomalies. Following Dessler et al. (2014), decadal regression terms are lagged in order to maximize MLR fit: we lag ΔT by 3 months, the BDC by 1 month, and the QBO by 3 months. These lags reflect the time between changes in each index and the impact on $[H_2O]_{entry}$.

Figure 5 shows the median $\pm$ one standard deviation of the ten decadal adjusted R^2 values generated by each CCM. The ensemble average is 0.61±0.25, with some spread among the models. Also plotted are the adjusted R^2 from two regressions of the tropical average Aura Microwave Limb Sounder (MLS) 82-hPa water vapor mixing ratio observations from Dessler et al. (2014). One regression uses Modern-Era Retrospective Analysis for Research and Applications reanalysis (MERRA) data (Rienecker et al., 2011) and the other uses European Centre for Medium-Range Weather Forecasts interim reanalysis (ERAI) (Dee et al., 2011) for the ΔT and BDC indices; the QBO index is standardized anomaly of monthly and zonally averaged equatorial 50-hPa winds obtained from the NOAA Climate Prediction Center (http://www.cpc.ncep.noaa.gov/data/indices). The MLS data covers the time period 2004-2014.

Many of the models have a range of adjusted R^2 values that overlap with the observational regression. However, of the models producing the smallest decadal adjusted R^2 values: these are the models that produced the poorest fits to long-term detrended $[H_2O]_{entry}$. In particular, CCSRNIES CNRM-CM5-3, and NIWA-UKCA, have the smallest adjusted R^2 values for both detrended and decadal $[H_2O]_{entry}$.

Figure 6 shows the median and one standard deviation of each coefficient (values are listed in table 4), along with the coefficients from the regression of the MLS data (taken from Table 1 of Dessler et al. (2014)). We find that the CCMs agree unanimously that increases in ΔT are associated with increased $[H_2O]_{entry}$, though the CCM ensemble tends to underestimate

5

the observational estimate. The only models that don't fall within both observational ranges are CCSRNIES, CMAM-CCMI, and CNRM-CM5-3.

In addition, the spread between the different decades for a single model tends to be small. The coefficient for individual models ranges from 0.01 to 0.4 ppmv K^{-1}, with an average of 0.15 ppmv K^{-1} and a standard deviation of 0.11 ppmv K^{-1}. This gives us some confidence that the comparison between the CCMs and one decade of observations is meaningful.

Figure 6 shows that there exists significant spread in the CCMs' decadal BDC regression coefficients. The coefficient for individual models ranges from -8.4 to 2.9 ppmv (K/Day)$^{-1}$, with an average of -3.55 ppmv (K/Day)$^{-1}$ and a standard deviation of 3.58 ppmv (K/Day)$^{-1}$. On all timescales, we expect a strengthening BDC should cool the TTL and reduce $[H_2O]_{entry}$, so the coefficient should be negative. We see that the median is indeed negative for all CCMs except for the CNRM-CM5-3 and NIWA-UKCA, both of which yield a positive median BDC coefficient (these models also generated positive BDC coefficients for the century analysis).

Comparing to observations, we find that the model ensemble does well. The CCSRNIES, CCSRNIES-MIROC-3.2, CMAM, CMAM-CCMI, LMDZrepro, MRI-ESM1r1, and WACCM decadal BDC regression coefficients fall within 95% confidence of MERRA, and only CCSRNIES-MIROC-3.2, LMDZrepro, and WACCM fall within 95% confidence interval of ERAI. As with the ΔT coefficient, the spread between the different decades for a single model tends to be small; this again gives us some confidence in our comparisons to analysis of a single decade of observations.

Figure 6 shows that, for all CCMs, the ensemble average decadal QBO coefficient is approximately 0 ppmv. But even those that do simulate a QBO, as seen in the century analysis, see little impact on $[H_2O]_{entry}$ from it, with an ensemble average of 0.02±0.03 ppmv. This is significantly smaller than the response to the QBO in the observations, and this appears to be a clear deficiency in the model ensemble.

Only CCSRNIES-MIROC3.2 and CMAM-CCMI decadal regressions produce QBO coefficients approaching those from both observational regressions. Again, CMAM-CCMI does not simulate a QBO, and it is not clear to us why the model does so well in this aspect of our analysis.

Previous studies found that the QBO significantly influences TTL temperatures and subsequently $[H_2O]_{entry}$ (Zhou et al., 2001; Geller et al., 2002; Liang et al., 2011), so the lack of response in the model ensemble appears to be a problem in the models. Previous studies have investigated this issue, finding that a higher vertical resolution within the stratosphere can help resolve the QBO's impact on the lower stratosphere (Rind et al., 2014; Anstey et al., 2016; Geller et al., 2016). Clearly, this needs to be investigated further.

Similar to both the trended and detrended regression analysis, we calculated standardized regression coefficients for the decadal regressions, and the values are listed in Table 4. Within most models, we see that the BDC, on decadal timescales, has the largest impact on $[H_2O]_{entry}$, with ΔT having a smaller impact.

5 Century and Decadal Regression Coefficient Comparison

One interesting question is whether the regression coefficients from the decadal analyses are related to regression coefficients from century regressions. To answer this, Figure 7 shows the coefficients from the trended century regressions of each CCM plotted against the median of the decadal regressions from the same CCM. Also shown is a linear least-squares fit to the points. For the ΔT coefficient, the best fit line is:

$$\beta(\Delta T, century) = 1.21 \pm 0.44 \beta(\Delta T, decade) + 0.13 \pm 0.08 \tag{2}$$

All uncertainties are 95% confidence intervals. Thus, the ΔT coefficients from the trended MLRs are slightly larger than those from the decadal MLRs. Using values of $\beta(\Delta T, decade)$ from MLS observations and this fit, we predict $\beta(\Delta T, century)$ of 0.50 ±0.06 and 0.55 ±0.08 ppmv K^{-1} for MERRA and ERAI regressions, respectively.

For the BDC coefficient, the best fit line is:

$$\beta(BDC, century) = 1.16 \pm 0.32 \beta(BDC, decade) + 0.56 \pm 1.56 \tag{3}$$

The BDC coefficients from the trended MLRs also have a slightly larger magnitude than those from the decadal MLRs. By fitting the observed values of $\beta(BDC, decade)$ through equation 3, we predict $\beta(BDC, century)$ values of $\beta(BDC, century)$ of -3.45 ±1.09 and -2.34 ±1.09 ppmv (K/Day)$^{-1}$ for MERRA and ERAI regressions, respectively.

For the QBO coefficient, the best fit line is:

$$\beta(QBO, century) = 0.75 \pm 0.40 \beta(QBO, decade) + 0.004 \pm 0.01 \tag{4}$$

The QBO coefficients from the trended MLRs are slightly smaller than those from the decadal MLRs. Again, using equation 4, we predict $\beta(QBO, century)$ values of 0.09 ±0.03 and 0.09 ±0.02 ppmv for MERRA and ERAI regressions, respectively.

6 Conclusions

Climate models predict that tropical lower-stratospheric humidity ($[H_2O]_{entry}$) will increase as the climate warms, with important implications for the chemistry and climate of the atmosphere. We demonstrated in this paper a new way to quantify the physical processes underlying these model trends. Our method is based on regressing CCM $[H_2O]_{entry}$ time series against three processes that have been shown to be important to $[H_2O]_{entry}$: tropospheric temperature (ΔT), the strength of the Brewer-Dobson circulation (BDC), and the phase of the QBO. Our approach provides more insight into model processes than simply comparing $[H_2O]entry$ to TTL temperatures.

We do this on two separate time-scales: 1) the 21st century, and 2) on decadal timescales. We find that long-term increase in $[H_2O]_{entry}$ in the CCMs is primarily driven by warming of the troposphere. This is partially offset in most CCMs by an increase in the strength of the Brewer-Dobson circulation, which tends to cool the tropical tropopause layer (TTL) (Randel et al., 2006; Fueglistaler et al., 2014). However, for the detrended data, we find a strengthening Brewer-Dobson circulation is of greater importance to the variability of $[H_2O]_{entry}$, consistent with Geller and Zhou (2007). The models show little impact

from the QBO, in disagreement with observations (O'Sullivan and Dunkerton, 1997; Randel et al., 1998; Dunkerton, 2001; Fueglistaler and Haynes, 2005; Choiu et al., 2006; Liang et al., 2011; Castanheira et al., 2012; Khosrawi et al., 2013; Kawatani et al., 2014; Tao et al., 2015); this appears to be a deficiency in the models.

The coefficients from regressions of individual decades in the CCMs can be compared to coefficients from regressions of observations covering a decade. Overall, the CCM ensemble seems to reproduce $[H_2O]_{entry}$ observations well, except for the fact that the CCMs simulate little response to the QBO, in disagreement with the observations. In addition, the good agreement on average hides some spread among the models, particularly in the response to the BDC.

Our overall conclusions are encouraging — the models appear to respond to the factors that control $[H_2O]_{entry}$ in realistic ways, providing some confidence in their simulations of $[H_2O]_{entry}$. However, some models have clear problems, e.g., the models that predict $[H_2O]_{entry}$ will increase with a strengthening BDC. In addition, nearly the entire ensemble does not reproduce the observed variations of $[H_2O]_{entry}$ with the phase of the QBO. This analysis should help the modeling groups refine their models' simulations of the 21st century.

7 Data availability

This data can be obtained through the British Atmospheric Data Center (BADC) archive.

References

Akiyoshi, H., Zhou, L. B., Yamashita, Y., Sakamoto, K., Yoshiki, M., Nagashima, T., Takahashi, M., Kurokawa, J., Takigawa, M., and Imamura, T.: A CCM simulation of the breakup of the Antarctic polar vortex in the years 1980–2004 under the CCMVal scenarios, Journal of Geophysical Research: Atmospheres, 114, n/a–n/a, doi:10.1029/2007JD009261, http://dx.doi.org/10.1029/2007JD009261, d03103, 2009.

Akiyoshi, H., Nakamura, T., Miyasaka, T., Shiotani, M., and Suzuki, M.: A nudged chemistry-climate model simulation of chemical constituent distribution at northern high-latitude stratosphere observed by SMILES and MLS during the 2009/2010 stratospheric sudden warming, Journal of Geophysical Research: Atmospheres, 121, 1361–1380, doi:10.1002/2015JD023334, http://dx.doi.org/10.1002/2015JD023334, 2015JD023334, 2016.

Anstey, J. A., Scinocca, J. F., and Keller, M.: Simulating the QBO in an Atmospheric General Circulation Model: Sensitivity to Resolved and Parameterized Forcing, J. Atmos. Sci., 73, 1649–1665, doi:10.1175/JAS-D-15-0099.1, 2016.

Brewer, A. W.: Evidence for a World Circulation Provided by the Measurements of Helium and Water Vapour Distribution in the Stratosphere., Q. J. R. Meteorol. Soc., 75, 351–363, doi:10.1002/qj.49707532603, 1949.

Castanheira, J. M., Peevey, T. R., Marques, C. A. F., and Olsen, M. A.: Relationships between Brewer-Dobson circulation, double tropopauses, ozone and stratosphere water vapor, Atmos. Chem. Phys., 12, 10 195–10 208, doi:10.5194/acp-12-10195-2012, 2012.

Choiu, E. W., Thomason, L. W., and Chu, W. P.: Variability of Stratospheric Water Vapor Inferred from SAGE II, HALOE, and Boulder (Colorado) Balloon Measurements., J. Climate, 19, 4121–4133, doi:10.1175/JCLI3841.1, 2006.

Dee, D. P., Uppala, S. M., Simmons, A. J., Berrisford, P., Poli, P., Kobayashi, S., Andrae, U., Balmaseda, M. A., Balsamo, G., Bauer, P., Bechtold, P., Beljaars, A. C. M., van de Berg, L., Bidlot, J., Bormann, N., Delsol, C., Dragani, R., Fuentes, M., Geer, A. J., Haimberger, L., Healy, S. B., Hersbach, H., Hólm, E. V., Isaksen, L., Kållberg, P., Köhler, M., Matricardi, M., McNally, A. P., Monge-Sanz, B. M., Morcrette, J.-J., Park, B.-K., Peubey, C., de Rosnay, P., Tavolato, C., Thépaut, J.-N., and Vitart, F.: The ERA-Interim reanalysis: configuration and performance of the data assimilation system, Quarterly Journal of the Royal Meteorological Society, 137, 553–597, doi:10.1002/qj.828, http://dx.doi.org/10.1002/qj.828, 2011.

Dessler, A. E., Schoeberl, M. R., Wang, T., Davis, S. M., and Rosenlof, K. H.: Stratospheric water vapor feedback, PNAS, 110, 18 087–18 091, doi:10.1073/pnas.1310344110, 2013.

Dessler, A. E., Schoeberl, M. R., Wang, T., Davis, S. M., Rosenlof, K. H., and Vernier, J. P.: Variations of stratospheric water vapor over the past three decades, J. Geophys. Res. Atmos., 119, 12 588–12 598, doi:10.1002/2014JD021712, 2014.

Deushi, M. and Shibata, K.: Development of a Meteorological Research Institute chemistry-climate model version 2 for the study of tropospheric and stratospheric chemistry, Papers in Meteorology and Geophysics, 62, 1–46, doi:10.2467/mripapers.62.1, 2011.

Donnelly, D.: The Fast Fourier Transform For Experimentalist, Part V: Filters., Computing in Science and Engineering, 8, 92–95, doi:10.1109/MCSE.2006.14, 2006.

Dunkerton, T.: On the Mean meridional mass motions of the stratosphere and mesosphere., J. Atmos. Sci., 58, 7–25, doi:10.1175/1520-0469(1978)035<2325:OTMMMM>2.0.CO;2, 2001.

Forster, P. M. d. F. and Shine, K. P.: Stratospheric water vapour changes as a possible contributor to observed stratospheric cooling, Geophysical Research Letters, 26, 3309–3312, doi:10.1029/1999GL010487, http://dx.doi.org/10.1029/1999GL010487, 1999.

Fueglistaler, S. and Haynes, P. H.: Control of interannual and longer-term variability of stratospheric water vapor, J. Geophys. Res., 110, doi:10.1029/2005JD006019, 2005.

Fueglistaler, S., B.Legras, Beljaars, A., Morcrette, J. J., Simmons, A., Tompkins, A. M., and Uppala, S.: The diabatic heat budget of the upper troposphere and lower/mid stratosphere in ECMWF reanalyses., Q. J. R. Meteorol. Soc., 135, 21–37, doi:10.1002/qj.361, 2009a.

Fueglistaler, S., Dessler, A. E., Dunkerton, T. J., Folkins, I., Fu, Q., and Mote, P. W.: Tropical tropopause layer, Rev. Geophys., 47, doi:10.1029/2008RG000267, 2009b.

5 Fueglistaler, S., Liu, Y. S., Flannaghan, T. J., Ploeger, F., and Haynes, P. H.: Departure from Clausius-Clapeyron scaling of water entering the stratosphere in response to changes in tropical upwelling, J. Geophys. Res. Atmos., 119, 1962–1972, doi:10.1002/2013JD020772, 2014.

Garcia, R. R., Marsh, D. R., Kinnison, D. E., Boville, B. A., and Sassi, F.: Simulation of secular trends in the middle atmosphere, 1950–2003, Journal of Geophysical Research: Atmospheres, 112, n/a–n/a, doi:10.1029/2006JD007485, http://dx.doi.org/10.1029/2006JD007485, d09301, 2007.

10 Geller, M. A. and Zhou, T.: Morphology of Tropical Upwelling in the Lower Stratosphere, J. Atmos. Sci., 65, 2360–2374, doi:10.1175/2007JAS2421.1, 2007.

Geller, M. A., Zhou, X., and Zhang, M.: Simulations of the Interannual Variability of Stratospheric Water Vapor, J. Atmos. Sci., 59, 1076–1085, doi:10.1175/1520-0469(2002)059<1076:SOTIVO>2.0.CO;2, 2002.

Geller, M. A., Zhou, T., Shindell, D., Ruedy, R., Aleinov, I., Nazarenko, L., Tausnev, N. L., Kelley, M., Sun, S., Cheng, Y., Field, R. D.,
15 and Faluvegi, G.: Modeling the QBO—Improvements resulting from higher- model vertical resolution, J. Adv. Model. Earth Syst., 8, doi:10.1002/2016MS000699, 2016.

Gilford, D. M., Solomon, S., and Portmann, R. W.: Radiative Impacts of the 2011 Abrupt Drops in Water Vapor and Ozone in the Tropical Tropopause Layer, J. Climate, 29, 595–612, doi:10.1175/JCLI-D-15-0167.1, 2016.

Imai, K., Manago, N., Mitsuda, C., Naito, Y., Nishimoto, E., Sakazaki, T., Fujiwara, M., Froidevaux, L., von Clarmann, T., Stiller, G. P.,
20 Murtagh, D. P., Rong, P.-p., Mlynczak, M. G., Walker, K. A., Kinnison, D. E., Akiyoshi, H., Nakamura, T., Miyasaka, T., Nishibori, T., Mizobuchi, S., Kikuchi, K.-i., Ozeki, H., Takahashi, C., Hayashi, H., Sano, T., Suzuki, M., Takayanagi, M., and Shiotani, M.: Validation of ozone data from the Superconducting Submillimeter-Wave Limb-Emission Sounder (SMILES), Journal of Geophysical Research: Atmospheres, 118, 5750–5769, doi:10.1002/jgrd.50434, http://dx.doi.org/10.1002/jgrd.50434, 2013.

IPCC: Climate Change 2001: The Scientific Basis: Contribution of Working Group 1 to the Third Assessment Report of the Intergovernmental
25 Panel on Climate Change, Tech. rep., Intergovernmental Panel on Climate Change (IPCC), New York, 2001.

Jonsson, A. I., de Grandpré, J., Fomichev, V. I., McConnell, J. C., and Beagley, S. R.: Doubled CO2-induced cooling in the middle atmosphere: Photochemical analysis of the ozone radiative feedback, Journal of Geophysical Research: Atmospheres, 109, n/a–n/a, doi:10.1029/2004JD005093, http://dx.doi.org/10.1029/2004JD005093, d24103, 2004.

Jourdain, L., Bekki, S., Lott, F., and Lefèvre, F.: The coupled chemistry-climate model LMDz-REPROBUS: description and evaluation of
30 a transient simulation of the period 1980–1999, Annales Geophysicae, 26, 1391–1413, doi:10.5194/angeo-26-1391-2008, http://www.ann-geophys.net/26/1391/2008/, 2008.

Kawatani, Y., Lee, J. N., and Hamilton, K.: Interannual Variations of Stratospheric Water Vapor in MLS Observations and Climate Model Simulations., J. Atmos. Sci., 71, 4072–4085, doi:10.1175/JAS-D-14-0164.1, 2014.

Khosrawi, F., Müller, R., Urban, J., Proffitt, M. H., Stiller, G., Kiefer, M., Lossow, S., Kinnison, D., Olschewski, F., Riese, M., and Murtagh,
35 D.: Assessment of the interannual variability and influence of the QBO and upwelling on tracer–tracer distributions of N_2O and O_3 in the tropical lower stratosphere, Atmos. Chem. Phys., 13, 3619–3641, doi:10.5194/acp-13-3619-2013, http://www.atmos-chem-phys.net/13/3619/2013/, 2013.

Liang, C. K., Eldering, A., Gettelman, A., Tian, B., Wong, S., Fetzer, E. J., and Liou, K. N.: Record of tropical interannual variability of temperature and water vapor from a combined AIRS-MLS data set, J. Geophys. Res. Atmos., 116, n/a–n/a, doi:10.1029/2010JD014841, http://dx.doi.org/10.1029/2010JD014841, d06103, 2011.

Manabe, S. and Wetherald, R. T.: Thermal Equilibrium of the Atmosphere with a Given Distribution of Relative Humidity, J. Atmos. Sci., 24, 241–259, doi:10.1175/1520-0469(1967)024<0241:TEOTAW>2.0.CO;2, 1967.

Maycock, A. C., Joshi, J. M., Shine, K. P., Davis, S. M., and Rosenlof, K. H.: The potential impact of changes in lower stratospheric water vapour on stratospheric temperatures over the past 30 years, Q. J. R. Meteorol. Soc., 26, doi:10.1002/qj.2287, 2014.

Meinshausen, M., Smith, S. J., Calvin, K., Daniel, J. S., Kainuma, M. L. T., Lamarque, J.-F., Matsumoto, K., Montzka, S. A., Raper, S. C. B., Riahi, K., Thomson, A., Velders, G. J. M., and van Vuuren, D. P. P.: The RCP greenhouse gas concentrations and their extensions from 1765 to 2300, Climatic Change, 109, 213–241, doi:10.1007/s10584-011-0156-z, 2011.

Michou, M., Saint-Martin, D., Teyssèdre, H., Alias, A., Karcher, F., Olivié, D., Voldoire, A., Josse, B., Peuch, V.-H., Clark, H., Lee, J. N., and Chéroux, F.: A new version of the CNRM Chemistry-Climate Model, CNRM-CCM: description and improvements from the CCMVal-2 simulations, Geoscientific Model Development, 4, 873–900, doi:10.5194/gmd-4-873-2011, http://www.geosci-model-dev.net/4/873/2011/, 2011.

Molod, A., Takacs, L., Suarez, M., Bacmeister, J., Song, I. S., and Eichmann, A.: The GEOS-5 Atmospheric General Circulation Model: Mean Climate and Development from MERRA to Fortuna, NASA Technical Report Series on Global Modeling and Data Assimilation, Tech. Rep. NASA TM-2012-104606, NASA GFSC, 2012.

Molod, A., Takacs, L., Suarez, M., and Bacmeister, J.: Development of the GEOS-5 atmospheric general circulation model: evolution from MERRA to MERRA2, Geoscientific Model Development, 8, 1339–1356, doi:10.5194/gmd-8-1339-2015, http://www.geosci-model-dev.net/8/1339/2015/, 2015.

Morgenstern, O., Braesicke, P., O'Connor, F. M., Bushell, A. C., Johnson, C. E., Osprey, S. M., and Pyle, J. A.: Evaluation of the new UKCA climate-composition model â€" Part 1: The stratosphere, Geoscientific Model Development, 2, 43–57, doi:10.5194/gmd-2-43-2009, http://www.geosci-model-dev.net/2/43/2009/, 2009.

Morgenstern, O., Giorgetta, M. A., Shibata, K., Eyhring, V., Waugh, D. W., Shepherd, T. G., Akiyoshi, H., Austin, J., Baumgaertner, A. J. G., Bekki, S., Braesicke, P., Brühl, C., Chipperfield, M. P., Cugnet, D., Dameris, M., Dhomse, S., Frith, S. M., Garny, H., Gettleman, A., Hardiman, S. C., Hegglin, M. I., Jöckel, P., Kinnison, D. E., Lamarque, J. F., Mancini, E., Manzini, E., Marchand, M., Michou, M., Nakamura, T., Nielsen, J. E., Olivié, D., Pitari, G., Plummer, D. A., Rozanov, E., Scinocca, J. F., Smale, D., Teyssèdre, H., Toohey, M., Tian, W., and Yamashita, Y.: Review of the formulation of present-generation stratospheric chemistry-climate models and associated external forcings, J. Geophys. Res., 115, doi:10.1029/2009JD013728, 2010.

Morgenstern, O., Zeng, G., Luke Abraham, N., Telford, P. J., Braesicke, P., Pyle, J. A., Hardiman, S. C., O'Connor, F. M., and Johnson, C. E.: Impacts of climate change, ozone recovery, and increasing methane on surface ozone and the tropospheric oxidizing capacity, Journal of Geophysical Research: Atmospheres, 118, 1028–1041, doi:10.1029/2012JD018382, http://dx.doi.org/10.1029/2012JD018382, 2013.

Morgenstern, O., Hegglin, M. I., Rozanov, E., O'Connor, F. M., Abrams, N. L., Akkyoshi, H., Archibald, A. T., Bekki, S., Butchart, N., Chipperfield, M. P., Deushi, M., Dhomse, S. S., Garcia, R. R., Hardiman, S. C., Horowitz, L. W., Jockel, P., Josse, B., Kinnison, D., Lin, M. Y., Mancini, E., Manyin, M. E., Marchand, M., Marecal, V., Michou, M., Pitari, L. D. O. N. G., Plummer, D. A., Revell, L. E., Saint-Martin, D., Schofield, R., Stenke, A., Stone, K., Sudo, K., Tanaka, T. Y., Tilmes, S., Yamashita, Y., Yoshida, K., and Zeng, G.: Review of the global models used within the Chemistry-Climate Model Initiative (CCMI), GMD, doi:10.5194/gmd-2016-199, 2017.

Mote, P. W., Rosenlof, K. H., McIntyre, M. E., Carr, E. S., Gille, J. C., Holton, J. R., Kinnersley, J. S., Pumphrey, H. C., III, J. M. R., and Waters, J. W.: An atmospheric tape recorder: The imprint of tropical tropopause temperatures on stratospheric water vapor, J. Geophys. Res. Atmos., 101, 3989–4006, doi:10.1029/95JD03422, 1996.

Oman, L. D., Ziemke, J. R., Douglass, A. R., Waugh, D. W., Lang, C., Rodriguez, J. M., and Nielsen, J. E.: The response of trop-
5   ical tropospheric ozone to ENSO, Geophysical Research Letters, 38, n/a–n/a, doi:10.1029/2011GL047865, http://dx.doi.org/10.1029/2011GL047865, l13706, 2011.

Oman, L. D., Douglass, A. R., Ziemke, J. R., Rodriguez, J. M., Waugh, D. W., and Nielsen, J. E.: The ozone response to ENSO in Aura satellite measurements and a chemistry-climate simulation, Journal of Geophysical Research: Atmospheres, 118, 965–976, doi:10.1029/2012JD018546, http://dx.doi.org/10.1029/2012JD018546, 2013.

10   O'Sullivan, D. and Dunkerton, T. J.: The influence of the quasi-biennial oscillation on global constituent distributions, J. Geophys. Res. Atmos., 102, 21 731–21 743, doi:10.1029/97JD01689, http://dx.doi.org/10.1029/97JD01689, 1997.

Pawson, S., Stolarski, R. S., Douglass, A. R., Newman, P. A., Nielsen, J. E., Frith, S. M., and Gupta, M. L.: Goddard Earth Observing System chemistry-climate model simulations of stratospheric ozone-temperature coupling between 1950 and 2005, Journal of Geophysical Research: Atmospheres, 113, n/a–n/a, doi:10.1029/2007JD009511, http://dx.doi.org/10.1029/2007JD009511, d12103, 2008.

15   Randel, W. J., Wu, F., Russell, J. M., Roche, A., and Waters, J. W.: Seasonal cycles and QBO variations in stratospheric CH4 and H2O observed in UARS HALOE data, J. Atmos. Sci., 55, doi:10.1175/1520-0469(1998)055<0163:SCAQVI>2.0.CO;2, 1998.

Randel, W. J., Wu, F., Vömel, H., Nedoluha, G. E., and Forster, P.: Decreases in stratospheric water vapor after 2001: Links to changes in the tropical tropopause and the Brewer-Dobson circulation, J. Geophys. Res. Atmos., 111, doi:10.1029/2005JD006744, 2006.

Rienecker, M., Suarez, M. J., Gelaro, R., Todling, R., Bacmeister, J., Liu, E., Bosilovich, M. G., Schubert, S. D., Takacs, L., Kim, G. K.,
20   Bloom, S., Chen, J., Collins, D., Conaty, A., and Silva, A. D.: MERRA: Nasa 's Modern-Era Retrospective Analysis for Research and Applications, J. Climate, 24, 3624–3648, doi:10.1175/JCLI-D-11-00015.1, 2011.

Rind, D., Jonas, J., Balachandran, N. K., Schmidt, G. A., and Lean, J.: The QBO in two GISS global climate models: 1. Generation of the QBO, Journal of Geophysical Research: Atmospheres, 119, 8798–8824, doi:10.1002/2014JD021678, http://dx.doi.org/10.1002/2014JD021678, 2014JD021678, 2014.

25   Santer, B. D., Wigley, T. M. L., Boyle, J. S., Gaffin, D. J., Hnilo, J. J., Nychka, D., Parker, D. E., and Taylor, K. E.: Statistical sig-nificance of trends and trend differences in layer-average atmospheric temperature time series, J. Geophys. Res., 105, 7337–7356, doi:10.1029/1999jd901105, 2000.

Scinocca, J. F., McFarlane, N. A., Lazare, M., Li, J., and Plummer, D.: Technical Note: The CCCma third generation AGCM and its extension into the middle atmosphere, Atmospheric Chemistry and Physics, 8, 7055–7074, doi:10.5194/acp-8-7055-2008, http:
30   //www.atmos-chem-phys.net/8/7055/2008/, 2008a.

Scinocca, J. F., McFarlane, N. A., Lazare, M., Li, J., and Plummer, D.: Technical Note: The CCCma third generation AGCM and its extension into the middle atmosphere, Atmospheric Chemistry and Physics, 8, 7055–7074, doi:10.5194/acp-8-7055-2008, http://www.atmos-chem-phys.net/8/7055/2008/, 2008b.

Shibata, K. and Deushi, M.: Long-term variations and trends in the simulation of the middle atmosphere 1980–2004 by the chemistry-
35   climate model of the Meteorological Research Institute, Annales Geophysicae, 26, 1299–1326, doi:10.5194/angeo-26-1299-2008, http://www.ann-geophys.net/26/1299/2008/, 2008.

Solomon, S., Rosenlof, K. H., Portmann, R. W., Daniel, J. S., Davis, S. M., Sanford, T. J., and Gian-Kasper, P.: Contributions of Stratospheric Water Vapor to Decadal Changes in the Rate of Global Warming, Science, 327, 1219–1223, doi:10.1126/science.1182488, 2010.

SPARC: SPARC CCMVal Report on the Evaluation of Chemistry-Climate Models, Tech. rep., Stratosphere-troposphere Processes and their role in climate (SPARC), http://www.sparc-climate.org/publications/sparc-reports/, 2010.

Tao, M., Konopka, P., Ploeger, F., Grooß, J.-U., Müller, R., Volk, C. M., Walker, K. A., and Riese, M.: Impact of the 2009 major sudden stratospheric warming on the composition of the stratosphere, Atmos. Chem. Phys., 15, 8695–8715, doi:10.5194/acp-15-8695-2015, http://www.atmos-chem-phys.net/15/8695/2015/, 2015.

Voldire, A., Sanchez-Gomez, E., y Melia, D. S., Decharme, B., Cassou, C., Sénési, S., Valcke, S., Beau, I., Alias, A., Chevallier, M., Déqué, M., Deshayes, J., Douville, H., Fernandez, E., Madec, G., Maisonnave, E., Moine, M. P., Planton, S., Saint-Martin, D., Szopa, S., Tyteca, S., Alkama, R., Belamari, S., Braun, A., Coquart, L., and Chauvin, F.: The CNRM-CM5.1 global climate model: description and basic evaluation, Climate Dynamics, 40, 2091–2121, doi:10.1007/s00382-011-1259-y, 2013.

WMO: Scientific Assessment of Ozone Depletion: 2006, Tech. Rep. 50, Global Ozone Research and Monitoring Project, Geneva, Switzerland, 2007.

WMO: Scientific Assessment of Ozone Depletion: 2014, Tech. Rep. 56, Global Ozone Research and Monitoring Project, Geneva, Switzerland, 2014.

Yukimoto, S., Yoshimura, H., Hosaka, M., Sakami, T., Tsujino, H., Hirabara, M., Tanaka, T. Y., Deushi, M., Obata, A., Nakano, H., Adachi, Y., Shindo, E., Yabu, S., Ose, T., and Kitoh, A.: Meteorological Research Institute Earth System Model Version 1 (MRI- ESM1) – Model Description, Tech. Rep. of MRI, Tech. Rep. 64, Meteorological Research Institude, 2011.

Yukimoto, S., Adachi, Y., Hosaka, M., Sakami, T., Yoshimura, H., Hirabara, M., Tanaka, T. Y., Shindo, E., Tsujino, H., Deushi, M., Mizuta, R., Yabu, S., Obata, A., Nakano, H., Koshiro, T., Ose, T., and Kitoh, A.: A new global climate model of the Meteorological Research Institute: MRI-CGCM3 – Model description and basic performance, J. Meteorol. Soc. Jpn., 90, 23–64, doi:10.2151/jmsj.2012-A02, 2012.

Zhou, X. L., Geller, M. A., and Zhang, M. H.: Tropical Cold Point Tropopause Characteristics Derived from ECMWF Reanalyses and Soundings, J. Climate, 14, 1823?–1838, doi:10.1175/1520-0442(2001)014<1823:TCPTCD>2.0.CO;2, 2001.

Table 1. CCMs used in this analysis. The resolution is listed as (lat x lon x number of pressure levels). 31 vertical levels indicates CCM data is given on isobaric levels, while CCMs simulating data on >31 levels are given on sigma (hybrid-pressure) levels

CCM	Resolution	Dataset	Contains QBO	Institution	Reference(s)
CCSRNIES	2.8° x 2.8° x 31	CCMVal-2	No	NIES, Tsukuba, Japan	Akiyoshi et al. (2009)
CCSRNIES-MIROC3.2	2.8° x 2.8° x 34	CCMI-1	Yes	NIES, Tsukuba, Japan	Imai et al. (2013); Akiyoshi et al. (2016)
CMAM	5.5° x 5.6° x 31	CCMVal-2	No	EC, Canada	Scinocca et al. (2008b)
CMAM-CCMI	3.7° x 3.8° x 71	CCMI-1	No	EC, Canada	Jonsson et al. (2004); Scinocca et al. (2008a)
CNRM-CM5-3	2.8° x 2.8° x 31	CCMI-1	No	Meteo-France; France	Voldire et al. (2013); Michou et al. (2011)
GEOSCCM	2.0° x 2.5° x 31	CCMVal-2	No	NASA/GSFC, USA	Pawson et al. (2008)
GEOSCCM-CCMI	2.0° x 2.5° x 72	CCMI-1	Yes	NASA/GSFC, USA	Molod et al. (2012, 2015); Oman et al. (2011, 2013)
LMDZrepro	2.5° x 3.8° x 31	CCMVal-2	No	IPSL, France	Jourdain et al. (2008)
MRI	2.8° x 2.8° x 31	CCMVal-2	Yes	MRI, Japan	Shibata and Deushi (2008)
MRI-ESM1r1	2.8° x 2.8° x 80	CCMI-1	Yes	MRI, Japan	Yukimoto et al. (2011, 2012); Deushi and Shibata (2011)
NIWA-UKCA	2.5° x 3.8° x 31	CCMI-1	Yes	NIWA, NZ	Morgenstern et al. (2009, 2013)
WACCM	1.9° x 2.5° x 31	CCMVal-2	No	NCAR, USA	Garcia et al. (2007)

Table 2. Coefficients (βs) from regressions of trended $[H_2O]_{entry}$ time series, and the change in $[H_2O]_{entry}$ resulting from each process (βSTD()), where STD() is the standard deviation of each trended process.

CCM	ΔT		BDC		QBO	
	$\beta_{\Delta T}$	$\beta_{\Delta T}$STD(ΔT)	β_{BDC}	β_{BDC}STD(BDC)	$\beta_{\Delta QBO}$	β_{QBO}STD(QBO)
CCSRNIES	0.06±0.01	0.08±0.02	-0.67±0.95	-0.01±0.02	1.7×10^{-2} ±0.01	7.9×10^{-3} ±0.006
CCSRNIES-MIROC3.2	0.40±0.06	0.39±0.06	-3.4±1.9	-0.11±0.06	3.5×10^{-2} ±0.04	2.2×10^{-2} ±0.02
CMAM	0.26±0.02	0.39±0.03	-5.7±1.1	-0.07±0.01	8.0×10^{-4} ±0.03	4.7×10^{-4} ±0.02
CMAM-CCMI	0.22±0.05	0.21±0.05	-3.8±2.6	-0.06±0.04	8.2×10^{-2} ±0.04	3.8×10^{-2} ±0.02
CNRM-CM5-3	0.27±0.13	0.26±0.13	3.7±5.4	0.09±0.13	1.9×10^{-2} ±0.07	4.9×10^{-3} ±0.02
GEOSCCM	0.38±0.03	0.37±0.03	-6.7±0.82	-0.21±0.03	-1.3×10^{-2} ±0.01	-3.2×10^{-3} ±0.003
GEOSCCM-CCMI	0.27±0.03	0.27±0.02	-6.6±0.96	-0.17±0.03	5.2×10^{-3} ±0.02	2.8×10^{-3} ±0.01
LMDZrepro	0.55±0.04	0.72±0.05	-8.3±2.1	-0.10±0.04	1.4×10^{-2} ±0.04	6.8×10^{-3} ±0.02
MRI	0.57±0.03	0.58±0.03	-12.±1.3	-0.34±0.04	-4.1×10^{-3} ±0.03	-2.0×10^{-3} ±0.01
MRI-ESM1r1	0.36±0.05	0.36±0.05	-3.1±1.4	-0.12±0.05	1.7×10^{-2} ±0.03	9.5×10^{-3} ±0.02
NIWA-UKCA	0.20±0.07	0.20±0.07	4.3±4.6	0.06±0.07	-1.0×10^{-2} ±0.07	-5.9×10^{-3} ±0.04
WACCM	0.24±0.04	0.21±0.03	-3.5±1.2	-0.05±0.02	1.5×10^{-2} ±0.03	4.7×10^{-3} ±0.008

The table is under the heading **Trended Regression**.

The units of ΔT, BDC, and QBO are ppmv K^{-1}, ppmv (K/Day)$^{-1}$, and ppmv, while the units of $\beta_{\Delta T}$STD(ΔT), β_{BDC}STD(BDC), and β_{QBO}STD(QBO) are all ppmv. The uncertainty is the 95% confidence interval.

Table 3. Coefficients (βs) from regressions of detrended $[H_2O]_{entry}$ time series, and the change in $[H_2O]_{entry}$ resulting from each process (βSTD()), where STD() is the standard deviation of each detrended process.

	Detrended Regression					
CCM	ΔT		BDC		QBO	
	$\beta_{\Delta T}$	$\beta_{\Delta T}$STD(ΔT)	β_{BDC}	β_{BDC}STD(BDC)	$\beta_{\Delta QBO}$	β_{QBO}STD(QBO)
CCSRNIES	0.05±0.02	0.02±0.006	-0.67±0.67	-7.1x10^{-3} ±0.005	1.7x10^{-2} ±0.01	3.6x10^{-3} ±0.003
CCSRNIES-MIROC3.2	0.30±0.05	0.08±0.01	-4.3±0.83	-0.08±0.02	2.8x10^{-2} ±0.01	1.7x10^{-2} ±0.009
CMAM	0.26±0.03	0.10±0.01	-5.3±0.84	-0.05±0.008	7.0x10^{-4} ±0.02	1.9x10^{-4} ±0.006
CMAM-CCMI	0.26±0.05	0.05±0.01	-3.7±1.1	-0.04±0.01	7.7x10^{-2} ±0.04	2.9x10^{-2} ±0.005
CNRM-CM5-3	0.19±0.05	0.08±0.01	0.20±1.1	2.5x10^{-3} ±0.01	-3.3x10^{-2} ±0.01	-7.1x10^{-3} ±0.003
GEOSCCM	0.31±0.04	0.08±0.009	-6.6±0.65	-0.09±0.009	-1.0x10^{-2} ±0.01	-1.9x10^{-3} ±0.002
GEOSCCM-CCMI	0.25±0.04	0.07±0.01	-7.1±0.71	-0.17±0.03	4.4x10^{-3} ±0.01	2.3x10^{-3} ±0.007
LMDZrepro	0.59±0.05	0.25±0.02	-5.4±1.1	-0.05±0.02	-5.5x10^{-3} ±0.03	-2.3x10^{-3} ±0.01
MRI	0.52±0.03	0.18±0.02	-11.±1.0	-0.24±0.02	-4.6x10^{-4} ±0.02	2.2x10^{-4} ±0.01
MRI-ESM1r1	0.33±0.05	0.09±0.01	-4.3±0.61	-0.10±0.01	5.5x10^{-3} ±0.01	3.0x10^{-3} ±0.007
NIWA-UKCA	0.15±0.08	0.04±0.02	2.9±1.6	0.04±0.02	-1.0x10^{-2} ±0.02	-5.9x10^{-3} ±0.01
WACCM	0.23±0.05	0.06±0.01	-3.5±0.80	-0.04±0.01	1.5x10^{-2} ±0.02	2.8x10^{-3} ±0.004

The units of ΔT, BDC, and QBO are ppmv K^{-1}, ppmv (K/Day)$^{-1}$, and ppmv, while the units of $\beta_{\Delta T}$STD(ΔT), β_{BDC}STD(BDC), and β_{QBO}STD(QBO) are all ppmv. The uncertainty is the 95% confidence interval.

Table 4. Median coefficients from the decadal regressions of $[H_2O]_{entry}$ monthly anomalies, and the change in $[H_2O]_{entry}$ resulting from each process (βSTD()), where STD() is the standard deviation of each decadal process.

Decadal Regressions						
CCM	ΔT		BDC		QBO	
	$\beta_{\Delta T}$	$\beta_{\Delta T}$STD(ΔT)	β_{BDC}	β_{BDC}STD(BDC)	$\beta_{\Delta QBO}$	β_{QBO}STD(QBO)
CCSRNIES	0.03±0.04	8.7x10^{-3} ±0.01	-1.23±1.34	-0.01±0.02	5.26x10^{-3} ±0.02	1.5x10^{-3} ±0.005
CCSRNIES-MIROC3.2	0.10±0.17	0.03±0.02	-3.29±1.44	-0.10±0.04	6.05x10^{-2} ±0.01	5.7x10^{-2} ±0.02
CMAM	0.19±0.09	0.05±0.03	-6.06±1.34	-0.07±0.02	2.75x10^{-3} ±0.03	9.4x10^{-4} ±0.004
CMAM-CCMI	0.01±0.10	3.5x10^{-3} ±0.02	-4.70±1.29	-0.07±0.03	6.13x10^{-2} ±0.01	3.0x10^{-2} ±0.02
CNRM-CM5-3	0.06±0.14	0.01±0.03	2.89±1.44	0.05±0.02	1.84x10^{-2} ±0.02	4.9x10^{-3} ±0.01
GEOSCCM	0.17±0.10	0.04±0.02	-6.31±1.19	-0.13±0.03	-1.47x10^{-2} ±0.03	-4.9x10^{-3} ±0.005
GEOSCCM-CCMI	0.11±0.16	0.02±0.03	-8.00±1.89	-0.18±0.06	2.42x10^{-2} ±0.02	1.8x10^{-2} ±0.01
LMDZrepro	0.31±0.19	0.11±0.08	-2.71±2.71	-0.07±0.05	1.27x10^{-2} ±0.01	-6.9x10^{-3} ±0.03
MRI	0.35±0.09	0.12±0.04	-8.78±2.91	-0.25±0.07	-6.56x10^{-3} ±0.06	4.6x10^{-3} ±0.03
MRI-ESM1r1	0.19±0.04	0.05±0.01	-4.72±0.71	-0.13±0.03	1.17x10^{-2} ±0.03	8.9x10^{-3} ±0.02
NIWA-UKCA	0.05±0.29	0.01±0.06	2.11±3.26	0.04±0.05	-1.88x10^{-2} ±0.04	-1.5x10^{-2} ±0.03
WACCM	0.15±0.12	0.03±0.03	-2.25±0.85	-0.05±0.02	3.84x10^{-2} ±0.03	9.1x10^{-3} ±0.007
MLS/ERAI	0.34±0.17	0.11±0.05	-2.5±0.83	-0.17±0.06	1.1x10^{-1} ±0.04	0.11±0.05
MLS/MERRA	0.30±0.20	0.11±0.07	-3.5±1.6	-0.15±0.07	1.2x10^{-1} ±0.05	0.12±0.06

The units of ΔT, BDC, and QBO are ppmv K^{-1}, ppmv (K/Day)$^{-1}$, and ppmv, while the units of $\beta_{\Delta T}$STD(ΔT), β_{BDC}STD(BDC), and β_{QBO}STD(QBO) are all ppmv. The uncertainty represents the variability (one standard deviation) in the set of coefficients produced by each CCM. For observations, the error bars represent 95% confidence.
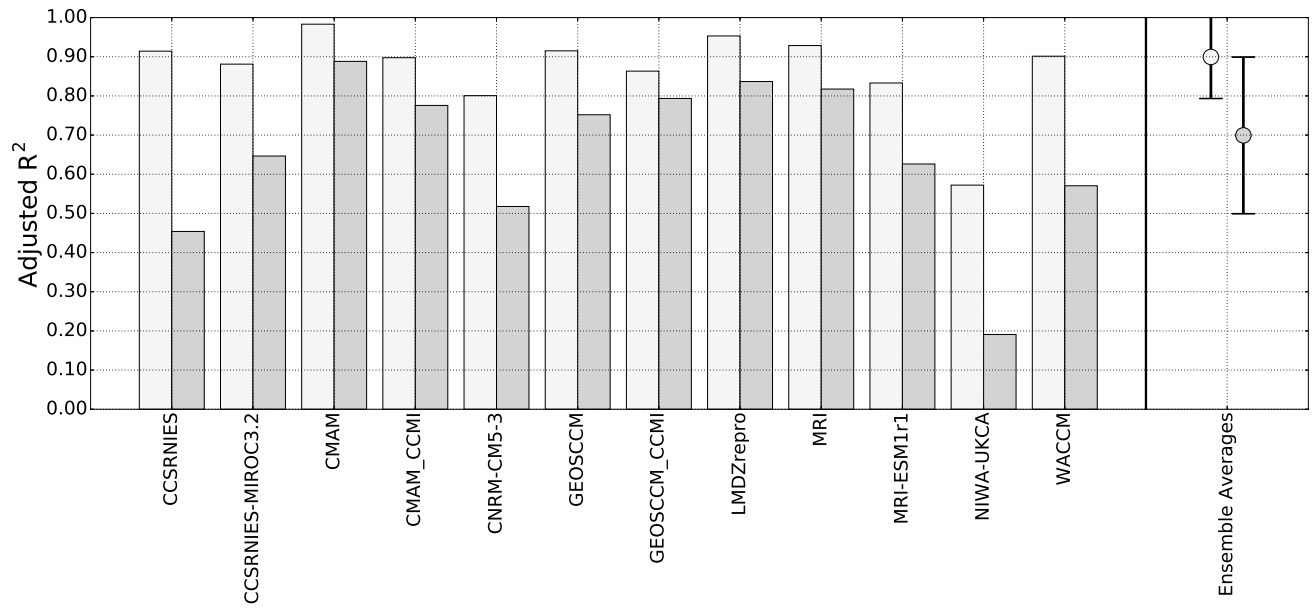
Figure 1. Bars corresponds to trended (light grey) and detrended (dark grey) adjusted R^2 values for annual-averaged data. The circles represent the ensemble mean, with error bars indicating $\pm$ one standard deviation of the CCM ensemble.
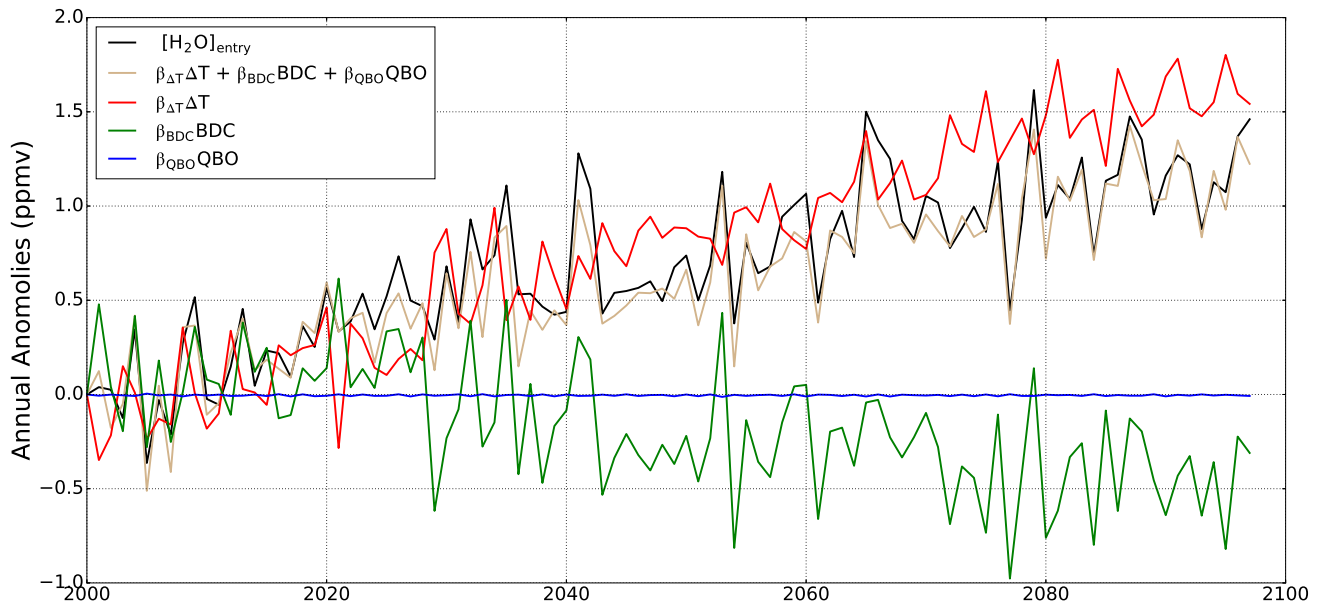
Figure 2. Time series of annual-averaged anomalies of $[H_2O]_{entry}$ from the MRI (black), and its reconstruction using a multivariate linear regression (brown). The red, green, and blue lines are the ΔT, BDC, and QBO terms from the regression, respectively.
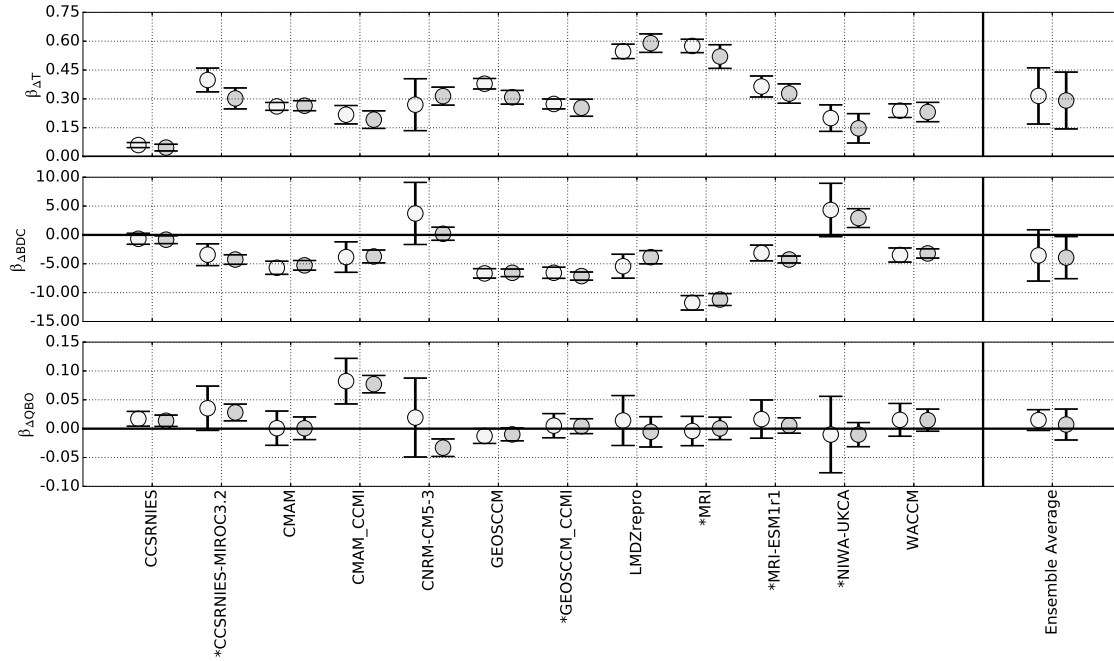
Figure 3. Circles show detrended (light grey) and trended (dark grey) coefficients for each model; error bars correspond to 95th percentile confidence interval bounding each regression coefficient. An asterisk indicates models simulating a QBO. The ensemble mean corresponds to the average of all model coefficients. The ensemble mean coefficients are also represented by a circle, with associated error bars correspond to $\pm$one standard deviation of the ensemble. The units of $\beta_{\Delta t}$, β_{BDC}, and β_{QBO} are ppmv/K, ppmv/(K/Day), and ppmv, respectively.
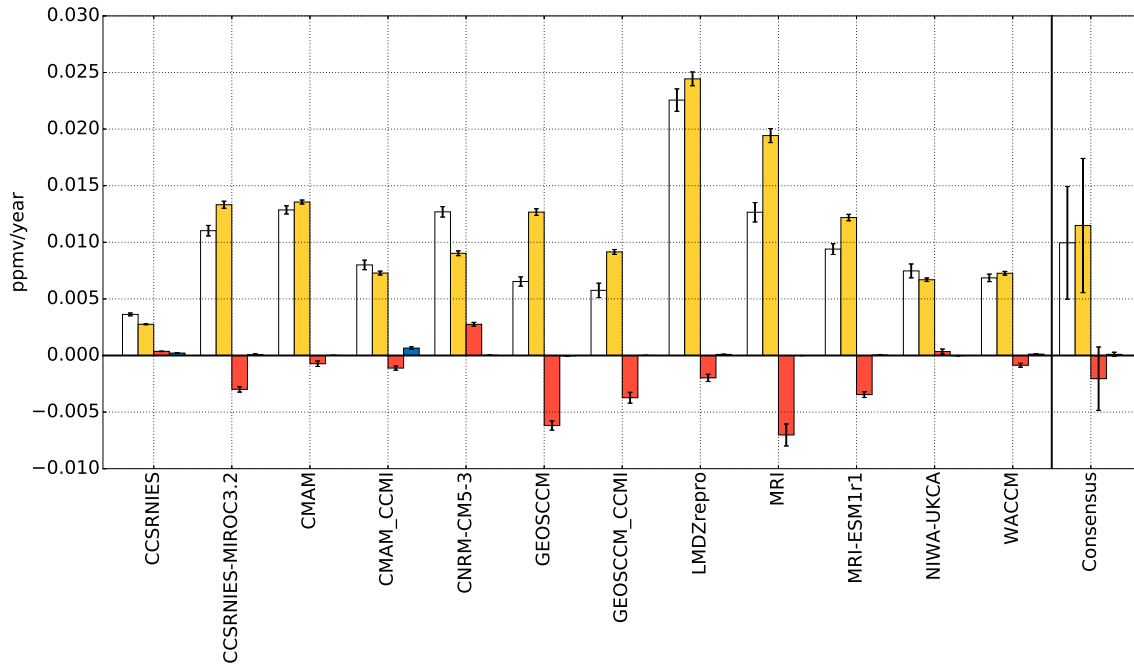
Figure 4. Trends in $[H_2O]entry$ resulting from ΔT (yellow), BDC (red), and QBO (blue) predictor time series assuming the other predictors are held constant. Each predictor trend is then compared to the trend of the full regression (white). Error bars represent 95% uncertainty. For many models, the contribution of the QBO is too small to be seen.
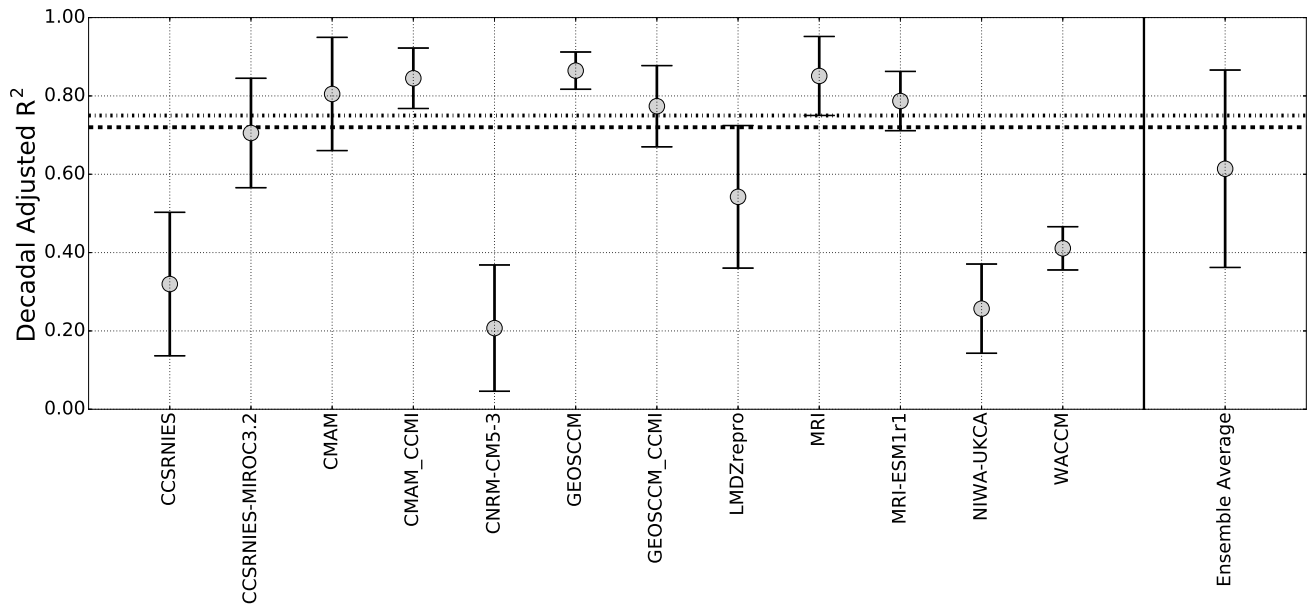
Figure 5. Circles represent the median of the adjusted R^2 value of the decadal fits. Errors correspond to the $\pm$ one standard deviation of the adjusted R^2 values. The CCM ensemble average is also plotted, along with error bars corresponding to $\pm$ one standard deviation of ensemble set of decadal adjusted R^2 values. The lines are adjusted R^2 values from observations combined with reanalysis (ERAI (dotted) and MERRA (dashed)) from Dessler et al. (2014).
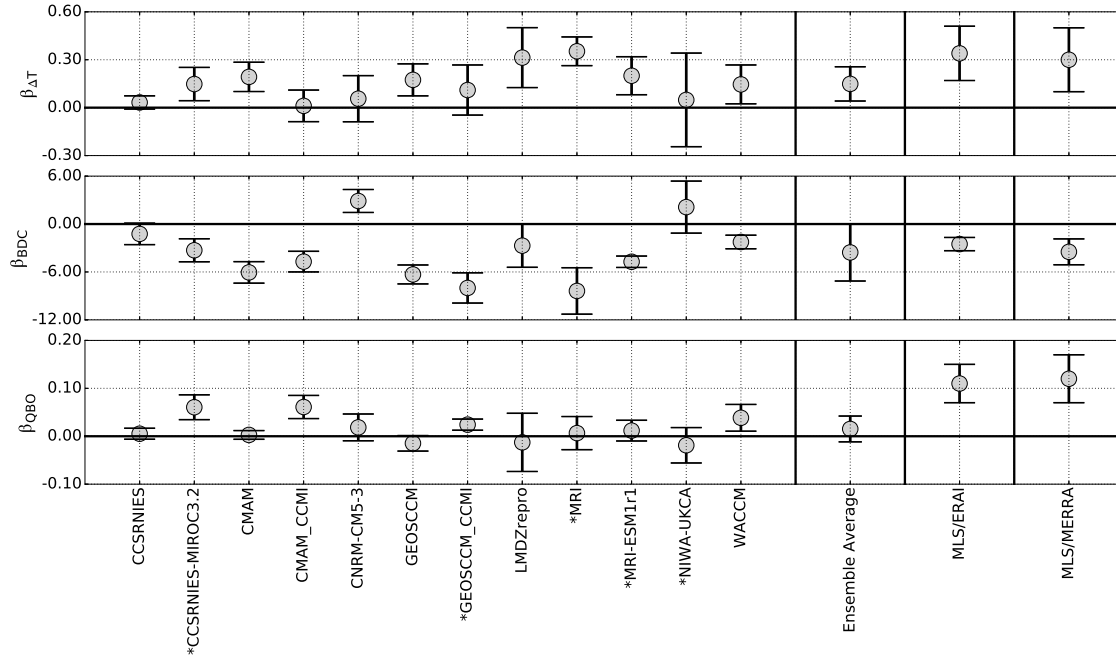
Figure 6. Circles represent the median decadal regression coefficient from each CCM, and error bars correspond to $\pm$ one standard deviation. An asterisk indicates that the model simulates a QBO. The ensemble mean corresponds to an average of all model coefficients. The ensemble mean coefficients are also represented by a circle, with associated error bars correspond to $\pm$one standard deviation of the ensemble set of coefficients. Estimates from observations combined with reanalysis (Dessler et al., 2014) shown, along with 95th percentile confidence interval. The units of $\beta_{\Delta t}, \beta_{BDC}$, and β_{QBO} are ppmv/K, ppmv/(K/Day), and ppmv, respectively.
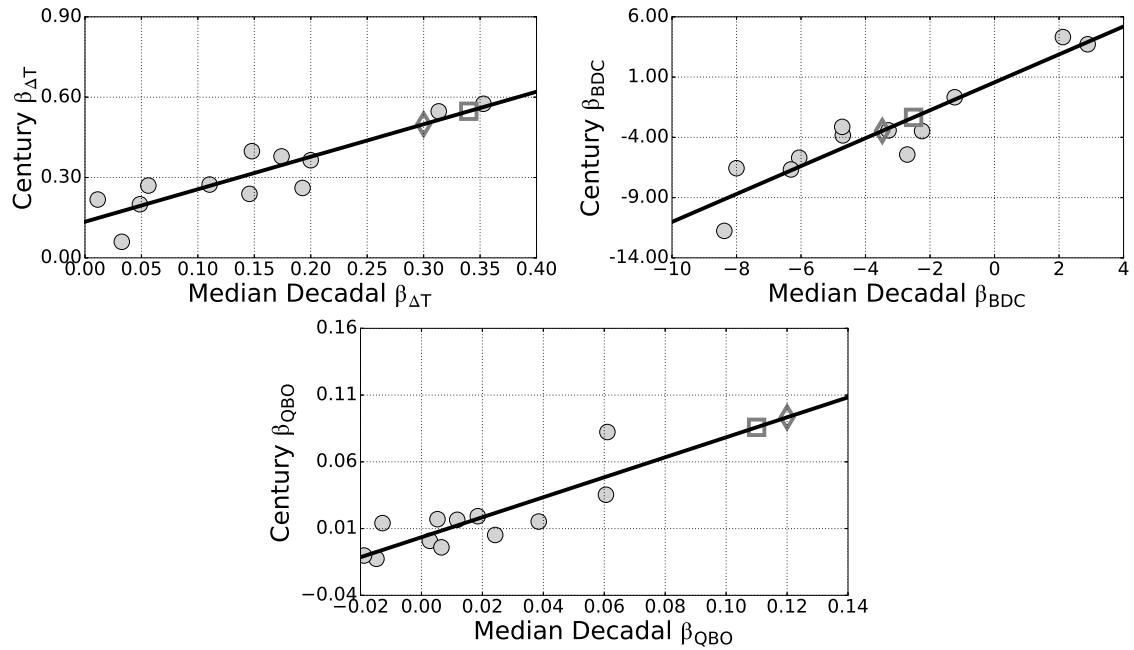
Figure 7. (Top Left) Scatter plots of trended ΔT regression coefficients (ppmv K^{-1}) vs. median decadal ΔT regression coefficients (ppmv K^{-1}) from each CCM. (Top Right) Same as top, but for BDC coefficients. (Bottom Middle) Same as top left and top right, but for QBO coefficient . Black lines in all plots correspond to a best fit line between the trended and decadal coefficients, and the observational coefficients ERAI (square) and MERRA (diamond) are fitted to each line (from Dessler et al. (2014)).